Biosensors and Bioelectronics 126 (2019) 581–589

Contents lists available at ScienceDirect

Biosensors and Bioelectronics

journal homepage: www.elsevier.com/locate/bios

A colorimetric immunosensor based on self-linkable dual-nanozyme for ultrasensitive bladder cancer diagnosis and prognosis monitoring

Chen Peng[a,1], Mu-Yi Hua[b,c,1], Nan-Si Li[a,d], Ying-Pei Hsu[a], Ying-Tzu Chen[a], Cheng-Keng Chuang[e,f], See-Tong Pang[e,f,*], Hung-Wei Yang[a,**]

[a] Institute of Medical Science and Technology, National Sun Yat-sen University, Kaohsiung 80424, Taiwan
[b] Department of Chemical and Materials Engineering, Biosensor Group, Biomedical Engineering Research Center; and Healthy Aging Research Center, Chang Gung University, Taoyuan 33302, Taiwan
[c] Department of Neurosurgery, Chang Gung Memorial Hospital, Linkou, Taoyuan 33305, Taiwan
[d] Institute of Biomedical Sciences, National Sun Yat-sen University, Kaohsiung 80424, Taiwan
[e] Division of Urology, Department of Surgery, Chang Gung Memorial Hospital, Linkou, Taoyuan 33305, Taiwan
[f] School of Medicine, Chang Gung University, Taoyuan 33302, Taiwan

ARTICLE INFO

Keywords:
Magnetic graphene oxide
Peroxidase mimicking
ApoA1 immunosensing
Signal amplification
Bladder cancer diagnosis

ABSTRACT

We developed self-linkable Prussian blue (PB)-incorporated magnetic graphene oxide (PMGO) as a peroxidase-mimicking nanozyme with high oxidizability to 3,3′,5,5′-tetramethylbenzidine (TMB), which generates significant absorption intensity for the colorimetric immunosensing of apolipoprotein A1 (ApoA1) in early bladder cancer (BC) diagnosis and prognosis monitoring. The ultrasensitive immunosensor was constructed using an ApoA1 antibody (Ab_{ApoA1})-functionalized chip ($biochip_{ApoA1}$) and self-linkable peroxidase-mimicking, PB-incorporated magnetic graphene oxide (PMGO). After incubating the sample and capturing ApoA1 proteins captured on the $biochip_{ApoA1}$, the PMGO was functionalized with Ab_{ApoA1}, and then mouse IgG (PMGO-1), rabbit anti-mouse IgG antibody (PMGO-2), and goat anti-rabbit IgG antibody (PMGO-3) were added together. We envisioned that each captured ApoA1 protein would allow the retention of a large amount of PMGO through a self-linking process to amplify the colorimetric signal of TMB in the presence of H_2O_2. The linear detection range could be obviously widened in the presence of self-linkable PMGO—from 0.05 ng/mL to 100 ng/mL—compared with the group without signal amplification (from 1 ng/mL to 100 ng/mL). Our immunosensor analysis of ApoA1 in the urine of BC patients and healthy individuals was highly correlated with enzyme-linked immunosorbent assay measurements; moreover, the ApoA1 concentrations of patients with high-grade BC were significantly higher than those of patients with low-grade BC. After standard clinical treatment, a significant drop of ApoA1 concentration occurred in urine that was lower than the cut-off concentration, suggesting potential clinical applications of the new self-linkable PMGO-generating colorimetric immunosensor in early BC diagnosis and prognosis monitoring.

1. Introduction

Bladder cancer (BC) is a tumor associated with high morbidity and mortality, and it is the fourth most common type of cancer (Siegel et al., 2018). The earlier that BC is found and treated, the better the outcome. Currently, cystoscopy is used as the gold standard for monitoring tumor diagnosis and progression as well as tumor recurrence; it is an invasive method associated with high costs and patient discomfort. Overall estimated costs for treatment and monitoring range between US$ 90,000 and US$ 200,000 per patient in the United States, because of the high recurrence rate and disease progression, which necessitates careful long-term monitoring (Yeung et al., 2014). Furthermore, it is the most expensive cancer to treat per patient. By contrast, urine cytology is specific and noninvasive for diagnosing BC, but it is limited by its poor sensitivity in low-grade tumors, which grow slowly and are less aggressive (Maas et al., 2018; Shao et al., 2017). Therefore, the invasiveness of cystoscopy and the limitations of cytology in detecting BC have generated the following critical goal for managing patients with

* Corresponding author at: Division of Urology, Department of Surgery, Linkou Chang Gung Memorial Hospital, Taoyuan 33305, Taiwan.
** Corresponding author.
E-mail addresses: jacobpang@cgmh.org.tw (S.-T. Pang), howardyang@mail.nsysu.edu.tw (H.-W. Yang).
[1] C. Peng and M.Y. Hua contributed equally to this work.

https://doi.org/10.1016/j.bios.2018.11.022
Received 5 September 2018; Received in revised form 28 October 2018; Accepted 14 November 2018
Available online 16 November 2018
0956-5663/

BC: to replace cystoscopy with the examination of voided urine, to reduce the frequency of cystoscopy. Voided urine can be collected more easily than other bodily fluids, such as blood and cerebrospinal fluid. Approximately 70% of urinary proteins are estimated to derive from the kidney and urinary tract, and abundant plasma proteins are present at high concentrations in urine specimens (Thomas et al., 2016; Chen et al., 2012). Cancer-related biomarkers (including circulating tumor protein and circulating tumor DNA/RNA) not only enable the detection of early stage tumors with high accuracy, but also the monitoring of tumor recurrence and progression, as well as the prediction of tumor response to therapeutic approaches (Kang et al., 2017). In cancer patients, free DNA in serum or urine is increased to a mean of 180 ng/mL compared with 13 ng/mL in healthy individuals, which is too low (pM concentration range) to accurately detect (Pursey et al., 2017). To date, a high content of mutated genes has been reported in patients with BC compared with healthy individuals. These genes are known as a tumor suppressor gene (*E. Cad*), a mediator of cell death (*DAPK*) and of cell growth gene (*RARβ*). Detection of these genes simultaneously in voided urine has been reported to diagnose BC with an accuracy of 90.9% and with a detection limit of 10 ng/mL (Yokoi et al., 2017). Moreover, FGFR3 (*S249C*) and HRAS (*G13R*) mutations are associated with low-grade bladder tumors; these mutations are mutually exclusive and occur in over 80% of low-grade tumors (Kompier et al., 2010; Leiblich, 2017).

In addition, tumor-specific proteins are potential biomarkers for early BC diagnosis and prognosis monitoring, a variety of candidate bladder cancer biomarkers such as RT112 cell CDH1, FHIT, LAMC2, RASSF1A, TIMP3, SFRP1, SOX9, PMF1, and RUNX3, have been identified but require further validation (Roberts et al., 2013; Kandimalla et al., 2013). Among them, apolipoprotein A1 protein (ApoA1), apolipoprotein A2 protein (ApoA2), and nuclear matrix protein 22 (NMP22) have recently been identified as a new biomarker that occurs at highly elevated rates in pooled BC. The relative difference in the levels of the abovementioned proteins in urine is a highly significant factor. The urinary level of ApoA1 in patients with BC is much higher than in normal people, indicating its potential utility in the development of a reliable BC detection assay (Chen et al., 2013; Tsai et al., 2018; Pichler et al., 2017). To date, an enzyme-linked immunosorbent assay (ELISA) is a commonly used traditional method to quantify the level of ApoA1 molecules in biofluids (Zell et al., 2016); however, the cost is relatively high and the enzyme used to catalyze H_2O_2 for producing signals—horseradish peroxidase (HRP)—is environmentally unstable (Garg et al., 2015). Therefore, various types of enzyme-mimicking nanomaterial have been developed to overcome the drawbacks of enzymes, because of their superior H_2O_2 catalyzing efficiency, high stability, and low costs, such as iron oxide (IO) (Tian et al., 2018a, 2018b), Prussian blue (PB) (He et al., 2017; Farka et al., 2018), MoS_2 (Hassanzadeh and Khataee, 2018), and G-quadruplex (G4) DNA-hemin complex (Li et al., 2018; Liu et al., 2018). Among them, the ferrous ions provided by IO or PB are widely utilized to catalyze H_2O_2-forming hydroxyl radical ($OH^·$), which can oxidize 3,3′,5′,5′-tetramethylbenzidine (TMB) as peroxidase-mimic materials.

Herein, we prepare the ApoA1 antibody (Ab_{ApoA1})-functionalized glassy chip ($biochip_{ApoA1}$) and peroxidase-mimicking, PB-incorporated magnetic graphene oxide (PMGO) with excellent environmental stability and self-chain linking reaction ability to construct an enzyme-free ultrasensitive immunosensor for accurately determining ApoA1 concentration in urine. Our colorimetric immunosensor with self-linkable PMGOs for signal amplification exhibits a rapid and sensitive ApoA1 detection with a wide linear detection range, which has potential for easy clinical BC diagnosis and prognosis monitoring.

2. Experimental methods

2.1. Preparation of ApoA1 antibody-modified glassy chip

To prepare the ApoA1 antibody (Ab_{ApoA1}; chicken host)-modified glassy chip for capturing ApoA1, a glassy chip with a diameter of 5 mm was first cleaned using a mixture of tris-buffered saline and Tween 20 (TBST), acetone, ethanol, and DI-H_2O. Subsequently, the cleaned chip was oxidized with HCl/methyl alcohol (volume ratio = 1:1) at 120 °C for 3 h to produce more hydroxide groups on the chip's surface. Next, the chip was soaked in APTES solution (10% in PBS buffer, pH 7.4) for 2 h to form a rich amine groups monolayer on the surface; the concentration of amine groups on the chip could be analyzed using TNBS assay. Subsequently, the chip was treated with glutaraldehyde (GA) in darkness for 2 h as a linker for Ab_{ApoA1} conjugation. After removing unreacted GA, the chip was incubated with 100 μL of Ab_{ApoA1} (2 μg/mL) for another 2 h in the dark. Finally, the Ab_{ApoA1}-modified chip was blocked using hexylamine and BSA to form $biochip_{ApoA1}$ that could be used to specifically capture ApoA1 (Fig. S1).

2.2. Preparation of PMGO

The graphene oxide (GO) was first synthesized using the modified Hummers' method (Stankovich et al., 2007). Briefly, graphite platelets (1 g), $NaNO_3$ (1 g), and H_2SO_4 (45 mL 98%) were magnetically mixed in a 250-mL flask in an ice bath, followed by the slow addition of 6 g of $KMnO_4$; the temperature was maintained below 5 °C. Subsequently, the flask was heated to 100 °C, followed by the slow addition of 100 mL of DI-H_2O. The temperature of the solution was increased to 98 °C for a 30 min incubation period; 35 mL of 10% H_2O_2 was added to the solution until the cessation of gas evolution. The solution was centrifuged at 10,000 rpm and washed several times with DI-H_2O to remove impurities and obtain GO.

Magnetic GO (MGO) composites were synthesized by coprecipitation of $FeCl_3$ and $FeCl_2{\cdot}4H_2O$ in the presence of GO. Briefly, 200 mg of GO in 20 mL of DI-H_2O was ultrasonicated for 30 min. $FeCl_3$ (175 mg) and $FeCl_2{\cdot}4H_2O$ (300 mg) were dissolved in 380 mL of DI-H_2O at room temperature, added to the GO solution, and stirred for 30 min under N_2 gas. The solution was heated slowly to 60 °C, and 10 mL of NaOH (17.5 mg/mL) was added over a 70 min period, after which the temperature was increased to 80 °C for 20 min. The solution was then rapidly quenched in ice and 0.1 N HCl was added slowly until the pH was neutral. MGO was separated from the solution by attraction to the wall of a separation funnel using a strong magnet, washed several times with DI-H_2O to remove unreacted material, and uniformly dispersed in DI-H_2O by sonication at 300 W for 1 h. To sufficiently conjugate the antibodies and adsorb Prussian blue (PB) to the MGO surface, MGO was modified with branched polyethylenimine (bPEI). An aqueous suspension of MGO was sonicated for approximately 30 min to obtain a clear solution; next, 24 mg of 1-Ethyl-3-(3-dimethylaminopropyl)-carbodiimide (EDC•HCl) and 27 mg of *N*-hydroxysulfosuccinimide sodium salt (sulfo-NHS) were dissolved in 2 mL of 0.5 M MES buffer (pH = 6.3) in the dark. A 0.2 mL aliquot of this solution was mixed with 0.2 mL of MGO (10 mg/mL) at 25 °C and sonicated for 30 min in the dark to allow the formation of amide bonds between activated carboxyl groups. Activated MGO was isolated, washed with 0.8 mL of 0.1 M MES buffer, resuspended in 0.2 mL of MES buffer, and then mixed with 0.2 mL of bPEI at 25 °C by vortexing for 2 h. Finally, it was washed three times with DI-H_2O to obtain bPEI-MGO.

Lastly, the bPEI-MGO was decorated with PB nanoparticles to exhibit excellent peroxidase activity. The synthesis process was as follows: 10 mL of PB precursor solution that contained 5 mM of $FeCl_3$ and 5 mM of $K_3[Fe(CN)_6]$ was prepared. After the pH value was adjusted to 1.5, the solution was mixed with preprepared bPEI-MGO at room temperature for 2 h. Under the acidic environment, the Fe^{3+} could be reduced to Fe^{2+} by GO, which immediately reacted with $Fe(CN)_6^{3-}$ to

form PB nanoparticles on the surface of the bPEI-MGO to obtain PMGO (Fig. S1).

2.3. Preparation of self-linkable PMGO

The proposed signal amplification strategy was accomplished through a self-linking reaction of three types of PMGO: PMGO-1, PMGO-2, PMGO-3. All antibodies were first modified with sulfenyl groups by reacting with excessive Traut's reagent in darkness for 1 h for further use. The PMGO-1 was synthesized as a capture probe to bind onto the ApoA1 captured on the biochip$_{ApoA1}$. The Ab$_{ApoA1}$ and mouse IgG were simultaneously conjugated on the PMGO; 1 mL of PMGO (20 μg/mL) was reacted with 33 μL of sulfosuccinimidyl 4-[*N*-maleimidomethyl] cyclohexane-1-carboxylate (sulfo-SMCC; 2 mg/mL) in darkness for 3 h and then reacted with thiol-functional Ab$_{ApoA1}$ and mouse IgG for another 2 h in darkness to obtain PMGO-1. The PMGO-2 and PMGO-3 were synthesized as signal-amplification probes to self-link to PMGO-1 and PMGO-2; 1 mL of PMGO (20 μg/mL) was reacted with 33 μL of sulfo-SMCC (2 mg/mL) in darkness for 3 h, and then reacted with thiol-functional rabbit anti-mouse IgG antibody (rabbit host) for another 2 h in darkness to obtain PMGO-2. Subsequently, 1 mL of PMGO (20 μg/mL) was reacted with 33 μL of sulfo-SMCC (2 mg/mL) in darkness for 3 h, and then reacted with thiol-functional goat anti-rabbit IgG antibody (goat host) for another 2 h in darkness to obtain PMGO-3. The obtained PMGO-1, PMGO-2, and PMGO-3 were blocked with 1% BSA to prevent nonspecific binding.

2.4. Colorimetric immunosensor for ApoA1 detection

For the detection process, various concentrations of ApoA1, ranging from 0.05 ng/mL to 100 ng/mL, were added into a tube containing biochip$_{ApoA1}$ and incubated for 30 min at room temperature. The ApoA1 was captured by Ab$_{ApoA1}$ because of the high affinity between them and the surface of the chips, which were gently washed three times with TBST. Subsequently, equal volumes (50 μL) of PMGO-1, PMGO-2, and PMGO-3 were added into the tube together and incubated for 30 min After washing with TBST, 100 μL of H_2O_2 + TMB as a developer was added into the tube for 3 min at room temperature, and then the oxidation was stopped by addition of HCl to show an absorption peak at 450 nm (Fig. S1). The produced yellow color of the solution became increasingly deep with increasing ApoA1 concentrations, and the $A_{450\,nm}$ was linearly proportional to the concentration of ApoA1. All experiments were conducted in sextuplicate for precise calculations to develop a standard protocol.

2.5. Interference tests

An outstanding immunosensor should possess not only specificity but also selectivity. Therefore, interference assays were conducted on our immunosensor. A variety of substances, such as urea (250 μg/mL), ascorbic acid (AA; 370 μg/mL), bovine serum albumin (BSA; 5%), fetal bovine serum (FBS, 10%), vascular endothelial growth factor (VEGF, 100 ng/mL), carbohydrate antigen 19–9 (CA19-9; 100 ng/mL), mucin 1 (MUC1; 100 ng/mL), and FXYD domain-containing ion transport regulator 3 (FXYD3; 100 ng/mL), were employed. First, the interferences or ApoA1 were added into the tube containing biochip$_{ApoA1}$, and the reaction was allowed to proceed for 30 min at room temperature. After the covering was rinsed gently with DI-H_2O three times, the washed biochip$_{ApoA1}$ was treated with 150 μL of self-linkable PMGOs (PMGO-1 + PMGO-2 + PMGO-3) for another 30 min, developing through the addition of 100 μL of H_2O_2 + TMB solution for 3 min at room temperature and then the addition of HCl to stop the reaction. The $A_{450\,nm}$ was recorded to determine the interference level using a SpectraMax M2 (Molecular Devices Co., California, USA).

2.6. Detection of ApoA1 in normal urine for recovery studies

Approximately 50 mL of clean-catch urine (the first morning mid-stream voided urine from healthy donors) conserved with 1 mM sodium azide as an antibacterial agent. The collected samples were immediately centrifuged at 1500 g, at 4 °C for 10 min. The urine was spiked with various concentrations of ApoA1 protein (20, 50, and 100 ng/mL) for recovery tests. In brief, 100 μL of urine solution spiked with ApoA1 at different concentrations was added to the tube containing biochip$_{ApoA1}$ and incubated for 30 min at room temperature; the biochip$_{ApoA1}$ was washed with TBST three times, and then incubated with 150 μL of self-linkable PMGOs (PMGO-1 + PMGO-2 + PMGO-3) for another 30 min developing through the addition of 100 μL of H_2O_2 + TMB solution and then the addition of HCl. The $A_{450\,nm}$ was recorded to determine the ApoA1 concentration in urine using the respective calibration curves for the colorimetric immunosensing using the SpectraMax M2. All recovery measurements were performed in triplicate for accurate calculations to develop a standard protocol.

2.7. Colorimetric immunosensor for BC diagnosis and prognosis monitoring

This study was approved by the Institutional Review Board of Chang Gung Memorial Hospital, Taiwan (IRB: 102–3642A3). Approximately 50 mL of clean-catch urine from four healthy donors and four patients with BC were immediately centrifuged at 1500 g, at 4 °C for 10 min. The sample for the immunosensor and ELISA analyses was collected from the supernatant and stored at − 80 °C. The seven urine samples from the patients with high-grade BC were collected before standard clinical treatment, three urine samples from the patients with low-grade BC were collected before standard clinical treatment, and six urine samples from the patients with high-grade BC were collected after standard clinical treatment and no recurrence was observed. For actual experiment, briefly, 100 μL of a urine sample was added to the tube containing biochip$_{ApoA1}$ which is fixed on the tube bottom then incubated for 30 min at room temperature; the biochip$_{ApoA1}$ was washed with TBST three times, and then incubated with excess of self-linkable PMGOs (50 μL PMGO-1 + 50 μL PMGO-2 + 50 μL PMGO-3) for another 30 min. The unbound PMGOs were washed out with TBST by shaking the tube, developing through the addition of 100 μL of H_2O_2 + TMB solution and then the addition of 10 μL HCl (1 M). The $A_{450\,nm}$ was recorded to determine the ApoA1 concentration in urine using the respective calibration curves for the colorimetric immunosensing. with the SpectraMax M2. Furthermore, we used a human ApoA1 ELISA kit (Arigo Biolaboratories Co., Taiwan), and followed the manufacturer's protocols to determine ApoA1 concentrations in human serum samples for comparison with the results from the immunosensor. All recovery measurements were performed in triplicate for accurate calculations to develop a standard protocol.

3. Results and discussion

3.1. Characterization and confirmation of prepared glassy biochips and PMGO

We envisioned a signal amplification approach to obtain a colorimetric immunosensor for determining ApoA1 concentration in patients' urine. The ultrasensitive immunosensor was constructed with biochip$_{ApoA1}$ and self-linkable peroxidase-mimic PMGO. After the samples were incubated and ApoA1 was captured on the biochip$_{ApoA1}$, the PMGO-1 was functionalized with Ab$_{ApoA1}$ and mouse IgG (PMGO-1), and then rabbit anti-mouse IgG antibody (PMGO-2) and goat anti-rabbit IgG antibody (PMGO-3) were added together. We envisioned that each captured ApoA1 protein should allow for the retention of a large amount of PMGO through a self-linking process, thereby oxidizing more H_2O_2 + TMB for the amplification of absorbance signals, as well as increasing the analytical performance of the immunosensor for ApoA1

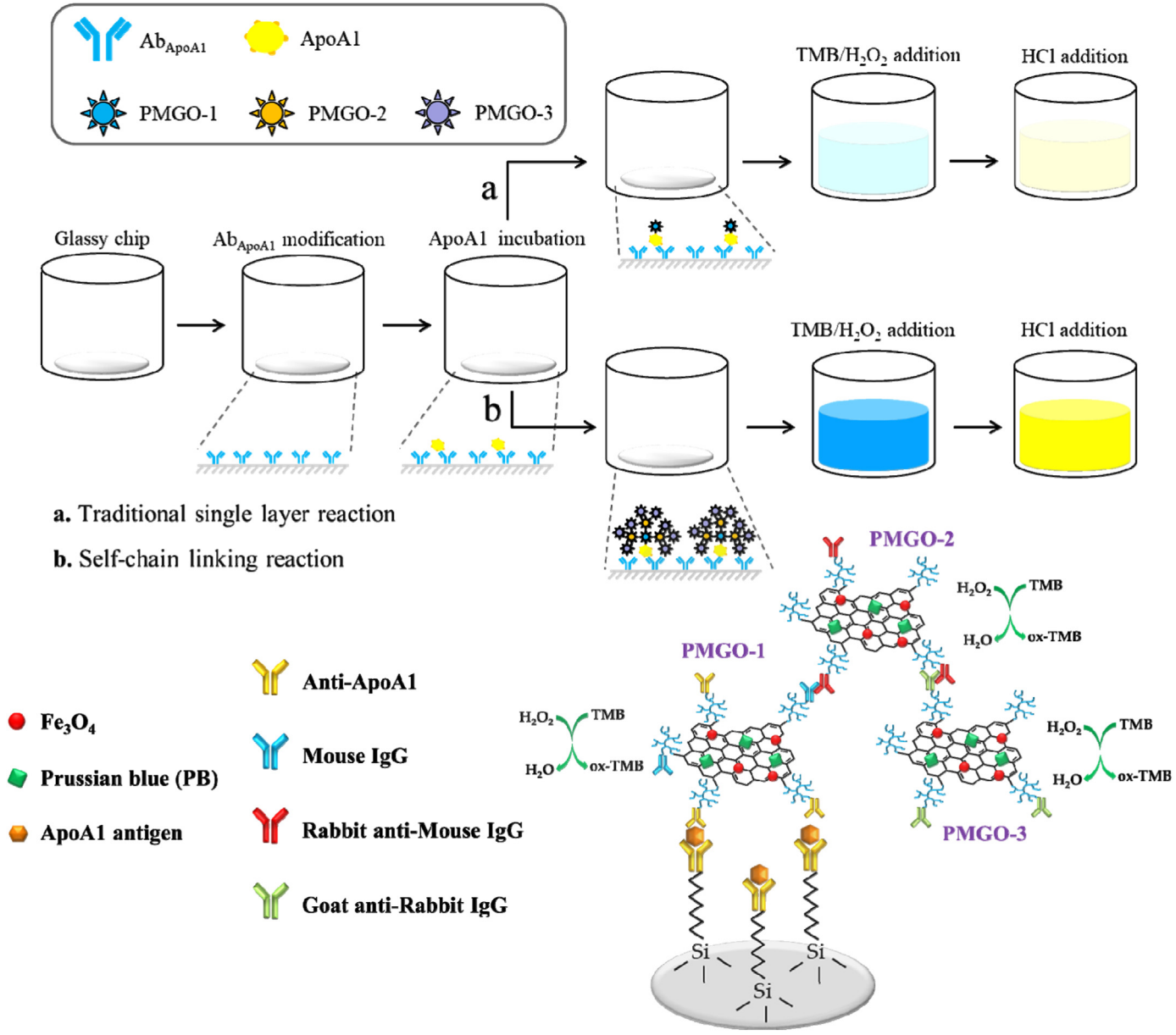

Fig. 1. Illustration of the ApoA1 detection procedures with (a) traditional signal and (b) self-chain linking reaction for signal amplification.

in early BC diagnosis and prognosis monitoring (Fig. 1).

The successful modification of amine groups on the surface of glassy chips was confirmed using a TNBS assay. We observed that the chips could be significantly stained with TNBS (thus showing a yellow color on their surface) when they were modified with APTES, indicating a large number of amine groups distributed well across the chips (Fig. 2A). The average roughness (R_a) increased to 0.22 nm from 0.16 nm, which was analyzed by AFM; this also confirmed that the APTES indeed covered the chips' surface (Fig. 2C). To determine whether the concentration of GA crosslinker affected the immobilization efficacy of Ab_{ApoA1}, the Ab_{ApoA1} concentration in the supernatant was analyzed by SDS-PAGE electrophoresis. The results showed that most of the Ab_{ApoA1} could be immobilized on the chip when the GA concentration was higher than 2%, and no free Ab_{ApoA1} remained in the supernatant (Lanes 5 and 6; Fig. 2B) compared with the control groups (Lanes 2 and 3; Fig. 2B) and lower GA concentration group (Lane 4; Fig. 2B). Also confirmed by AFM was that the R_a further increased to 4.95 nm with the Ab_{ApoA1} bound to the amine groups by GA on the chips from 0.22 nm, indicating that Ab_{ApoA1} immobilization on the chips by GA was successful in forming a biochip$_{ApoA1}$ (Fig. 2C). Subsequently, we incubated the biochip$_{ApoA1}$ with ApoA1 and then FITC-labeled Ab_{ApoA1}, and significant green fluorescence was exhibited on the chips' surface after washing with DI-H_2O_2, indicating that the immobilization procedure would not affect the Ab_{ApoA1} activity and the immobilized Ab_{ApoA1} can specifically capture ApoA1 (Fig. 2D).

The GO prepared using the Hummers' method was incorporated with IO to form MGO, which was further modified with bPEI (bPEI-MGO) to enhance the solubility and conjugating rate of MGO, as well as foster the attachment of PB nanoparticles. Finally, the bPEI-MGO was incorporated with PB to form PMGO as a peroxidase-mimicking nanozyme with high stability for ultrasensitive H_2O_2 + TMB oxidization. Next, we utilized zeta potential analysis, TEM, EDS, UV–vis spectra, FT-IR, XRD, and a SQUID to prove the successful preparation of each step.

The zeta potential decreased to − 70.4 ± 1.7 mV from − 19.7 ± 2.4 mV (GO) after chemical coprecipitation of IO nanoparticles, most likely because the negative charged IO nanoparticles were deposited onto the GO surface. This changed to + 41.5 ± 3.2 mV after modification with bPEI and then decreased to + 32.8 ± 7.3 mV after

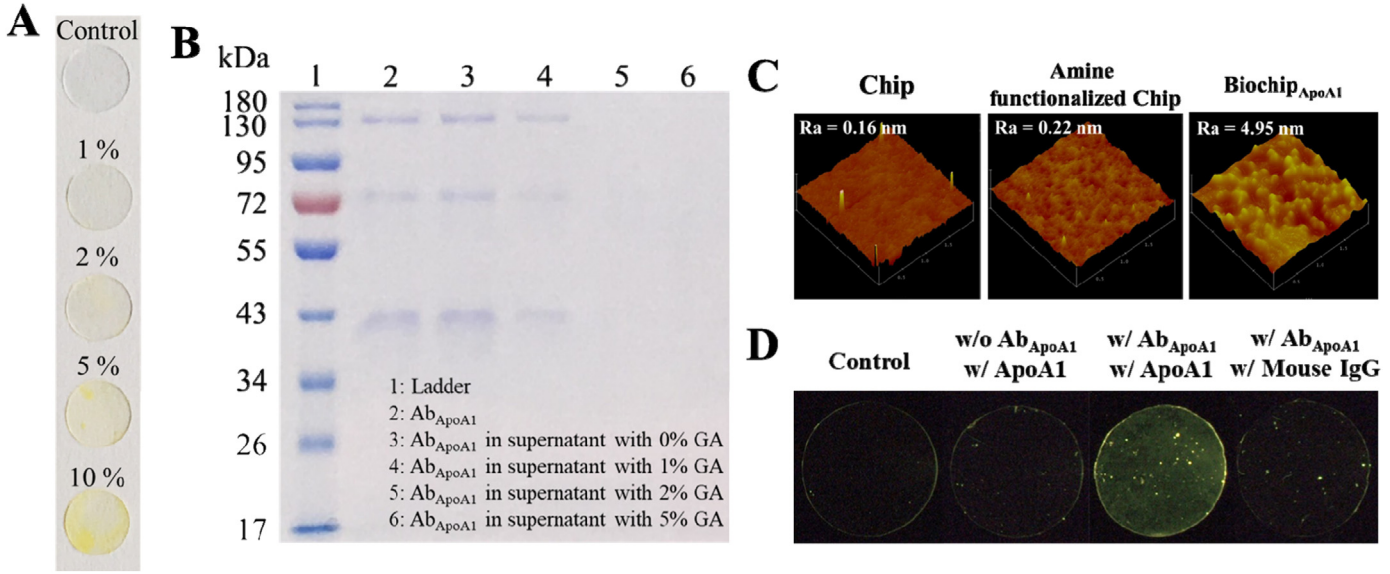

Fig. 2. (A) Quantification of amine groups (-NH_2) on chips using TNBS staining modified with 0 (negative control), 1%, 2%, 5%, and 10% APTES, respectively. (B) Analysis of the optimal conjugation rate of Ab_{ApoA1} on $biochip_{ApoA1}$ using different GA concentrations using SDS-PAGE Gel 12%. (C) AFM images of a pure glassy chip, amine-functionalized chip, and $biochip_{ApoA1}$. (D) Fluorescent image of ApoA1 captured $biochip_{ApoA1}$ stained with FITC-labeled Ab_{ApoA1}.

the incorporation of PB nanoparticles, indicating the successful formation of PMGO (Fig. S2).

The sheet size of GO was 700 ± 56 nm in width and 1000 ± 73 nm in length as determined by TEM. A closer examination revealed IO nanoparticles attached to the surface of MGO sheets, with sphere-like morphology and a size of 10.5 ± 3.2 nm. More dots with sphere-like morphology and a size of 21.8 ± 2.7 nm were observed to be distributed on the bPEI-MGO after the incorporation of PB nanoparticles (Fig. 3A). During EDS, a new Fe signal belonging to IO nanoparticles appeared after the IO nanoparticle attachment was compared with GO. Furthermore, a new N signal belonging to bPEI appeared after bPEI modification (Fig. 3B). The UV–vis spectrum of the resulting PMGO solution showed a shoulder peak at approximately 400 nm, which was attributed to the charge transfer from nitrogen to the metal center as a result of introducing IO nanoparticles, as well as a broad absorption with λ_{max} at 680 nm, which is consistent with an intermetal charge-transfer band from Fe^{2+} to Fe^{3+} in PB nanoparticles (Fig. 3C) (Zhao et al., 2018). This also confirmed the formation of PMGO.

Finally, SQUID analysis was performed to prove the successful deposition of nanoparticles and bPEI modification on the GO surface (Fig. 3D). The saturation magnetization of MGO was 70.9 emu/g compared with 0 emu/g for GO. This decreased to 57.2 emu/g after bPEI modification and then further decreased to 35.6 emu/g after PB nanoparticle deposition because of the proportional decrease of IO nanoparticles per unit weight in each step; however, it was high enough to allow guidance by an external magnet for easy and rapid purification (Fig. 3D; inset).

3.2. Comparison of peroxidation activity and stability of PMGO with HRP

Most relevant literature has indicated the high peroxidation activity of an HRP weak acid environment based on the H_2O_2 + TMB oxidation reaction; however, it may not suit all biomolecules. Thus, the influence of pH was investigated to determine the optimal experiment parameters for HRP and PMGO. A series of PBS solutions with pH values varying from 3 to 11 were prepared to explore the effect of pH on HRP and PMGO. The results in Fig. 4A indicate that the peroxidation activity of HRP is sensitive to pH and the optimal result was obtained under a pH of 6; the activity gradually decreased when the pH was higher or lower 6. By contrast, the peroxidation activity of PMGO was not affected by pH; the artificial enzyme PMGO could effectively oxidize H_2O_2 + TMB to obtain a consistent signal over a wide pH range from 3 to 11, indicating that PMGO is more suitable than HRP for the analysis of clinical samples. Therefore, unless stated specifically, a pH of 7.4 was used in subsequent experiments for PMGO.

Next, we investigated the oxidization ability of PMGO compared with that of HRP. The absorption intensity was set at 450 nm ($A_{450\ nm}$) of TMB, which was a similar level (approximately 0.75) after oxidization by HRP and PMGO, and then the $A_{450\ nm}$ values of TMB oxidized by HRP and PMGO at different dilutions were compared. From the results in Fig. 4B, the $A_{450\ nm}$ values of TMB decreased with the increase of dilution ratio in the range from 1 to 1024-fold, and the produced values for HRP and PMGO were similar at different dilution ratios, which indicated that PMGO has excellent catalysis ability toward H_2O_2 as HRP. The most common and serious problem of enzyme-based biosensors is their lack of stability because of the intrinsic nature of the enzyme. Thus, we evaluated the long-term stability of HRP and PMGO after a period of storage between 1 and 90 days at 25, 37, and 5 °C; the responses were monitored by reacting H_2O_2 + TMB with the HRP and PMGO stored at each time point. As seen in Fig. 4C, the HRP lost its complete activity after 7 days of storage at 50 °C, and could not maintain its activity beyond 40 days of storage at 25 °C. However, the PMGO was used for oxidization of H_2O_2 + TMB without any loss in sensitivity, even when stored at 25 and 37 °C for 90 days. Impressively, the PMGO can maintain its complete catalytic activity without any decay until 30 days of storage at 50 °C, and only 44.6% of the initial activity was lost after 90 days of storage, which is unmatched by HRP. To clearly understand why the catalytic activity of PMGO decayed at high temperature for a long period of storage, the PMGO was incubated at 70 °C for 7 days. From the results in Fig. 4D, the shoulder peak at approximately 400 nm attributed to IO nanoparticles still remained, but the absorbance peak at 680 nm attributed to PB nanoparticles disappeared. This means that the amount of PB nanoparticles on the PMGO decreased; however, to our knowledge based on the relevant literature, PB should not be decomposed from the PMGO surface at 70 °C because the isothermal decomposition temperature is approximately 350 °C (Machala et al., 2013). Therefore, we presumed that the PB nanoparticles may depart from the PMGO surface, resulting in the decrease of oxidization activity of PMGO to H_2O_2 + TMB. Based on these data, the peroxidase-mimicking dual nanozyme described herein

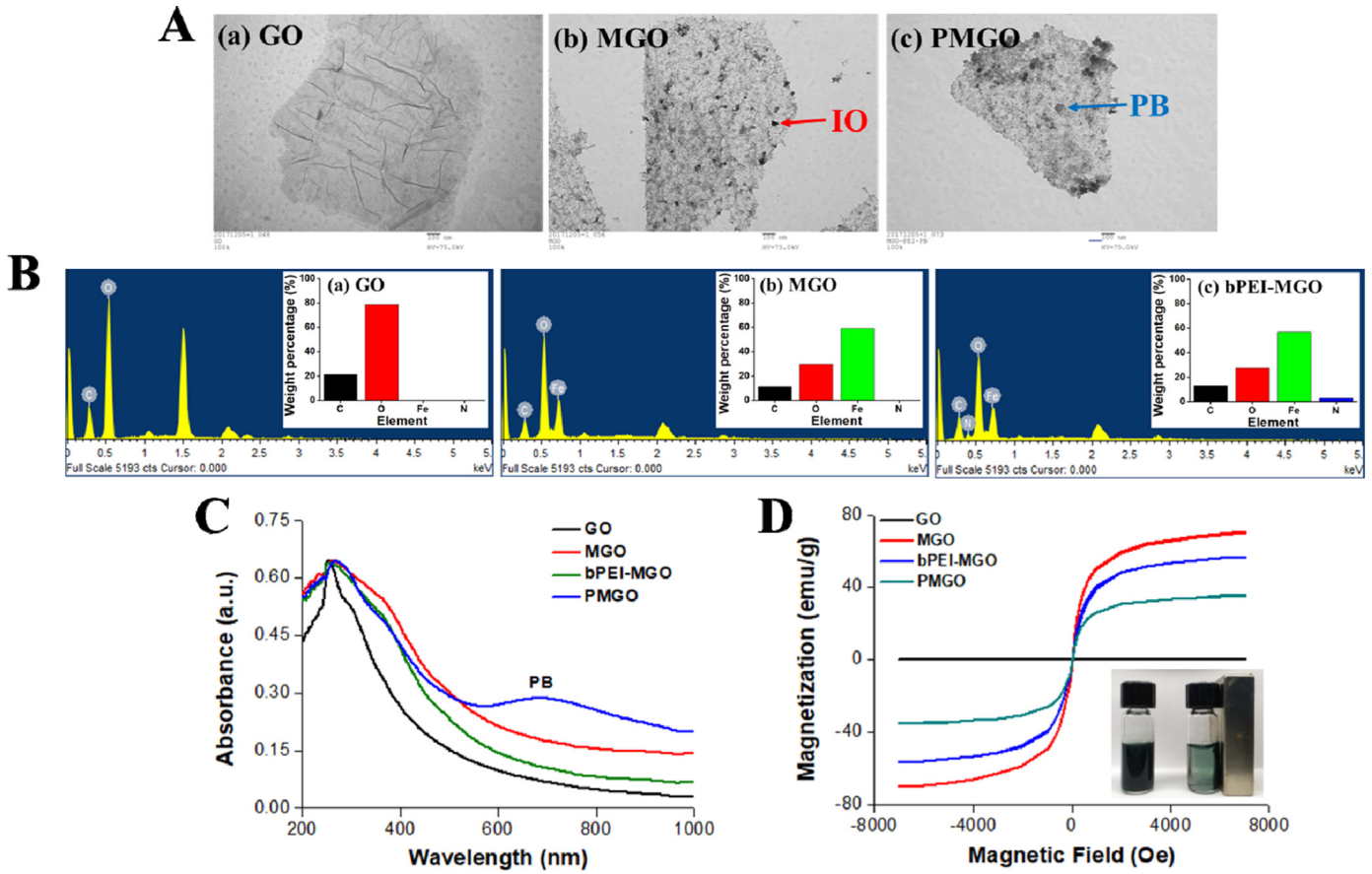

Fig. 3. (A) TEM images of GO, MGO, and PMGO. (B) EDS spectra of GO, MGO, and bPEI-MGO. (C) UV–vis spectra of GO, MGO, bPEI-MGO, and PMGO; the absorbance peak at 680 nm is attributed to PB. (D) Magnetic hysteresis curves of GO, MGO, bPEI-MGO, and PMGO nanocomposites at room temperature; the inset is a digital photo of the PMGO suspension with and without an exterior magnetic field.

presents high oxidization activity to H_2O_2 + TMB, strong thermal stability, and low cost, thereby making it suitable for replacing HRP as the signal for colorimetric immunosensing.

3.3. Confirmation of prepared self-linkable PMGO and signal amplification test

To make self-linkable PMGO for signal amplification, the PMGO was modified with various antibodies to form three types of PMGO: (i) PMGO-1 modified with Ab_{ApoA1} and mouse IgG; (ii) PMGO-2 modified with rabbit anti-mouse IgG antibody; and (iii) PMGO-3 modified with goat anti-rabbit IgG antibody. Subsequently, we analyzed the amount of antibodies in supernatants after the modification process to confirm the successful modification of antibodies on PMGO. From the results in Fig. 4E, no obvious bands were present in Lane 4 (compared with Lanes 2 and 3), Lane 6 (compared with Lane 5), or Lane 8 (compared with Lane 7), indicating that most of the antibodies were conjugated on the PMGO to form PMGO-1, PMGO-2, and PMGO-3 for self-signal amplification. Next, we constructed the immunosensor to prove the self-linking feasibility of PMGO. PMGO-1 could bind to the biochip in the presence of ApoA1 to catalyze H_2O_2 + TMB; the $A_{450\ nm}$ was 0.21 and exhibited a primrose yellow color (Fig. 4F(a)). As seen in Fig. 4F(c), the color became darker when the self-linkable signal (PMGO-1 + PMGO-2 + PMGO-3) was placed into the assay tube; the $A_{450\ nm}$ was significantly increased to 0.73 from 0.21 in the presence of the same concentration of ApoA1. The results indicated that the self-linkable PMGO is workable; PMGO-1 can efficiently bind to captured ApoA1, PMGO-2 can automatically link with PMGO-1, and PMGO-3 can automatically link with PMGO-2 to greatly amplify the colorimetric signal.

3.4. Colorimetric immunoassay of ApoA1 protein

The urinary levels of ApoA1 in patients with BC is much higher than in normal people (cut-off concentration = 11.16 ng/mL), indicating its potential utility in developing reliable BC diagnosis and prognosis monitoring (Chen et al., 2013; Tsai et al., 2018). Therefore, the detection range of an immunosensor for ApoA1 must be wide as possible. We compared the sensitivity and detection range of the immunosensor with and without self-signal amplification reactions. The standard curve was found to be linear and in the range of 1 ng/mL to 100 ng/mL for ApoA1 using PMGO-1 as the signal (r^2 = 0.991; Fig. 5A and D). Although the detection range covers the cut-off concentration of ApoA1 in urine to sufficiently determine the suffering risk of BC, the lowest limit of quantitation (LLOQ) should be lower because the concentration of ApoA1 may be lower than 1 ng/mL for patients receiving surgical operation and chemotherapy. Thus, we designed a simple signal amplification mechanism using self-linkable PMGOs as the signal amplifier to specifically recognize the ApoA1 for signal amplification. The standard curve was found to be linear, and the LLOQ was lowered to 0.2 ng/mL in the presence of PMGO-1 + PMGO-2 for a self-linking reaction (Fig. 5B and D). Impressively, the linear detection range could be obviously widened in the presence of PMGO-1 + PMGO-2 + PMGO-3, 0.05 ng/mL to 100 ng/mL, and its sensitivity was also much higher than the group with no signal amplification (Fig. 5C and D), which is sufficient for use in BC diagnosis and prognosis monitoring. The results demonstrated that PMGO-1 could bind to captured ApoA1 on the biochip, and PMGO-2 and PMGO-3 could automatically link to PMGO-1 and PMGO-2, respectively, to catalyze more H_2O_2 + TMB for colorimetric signal amplification.

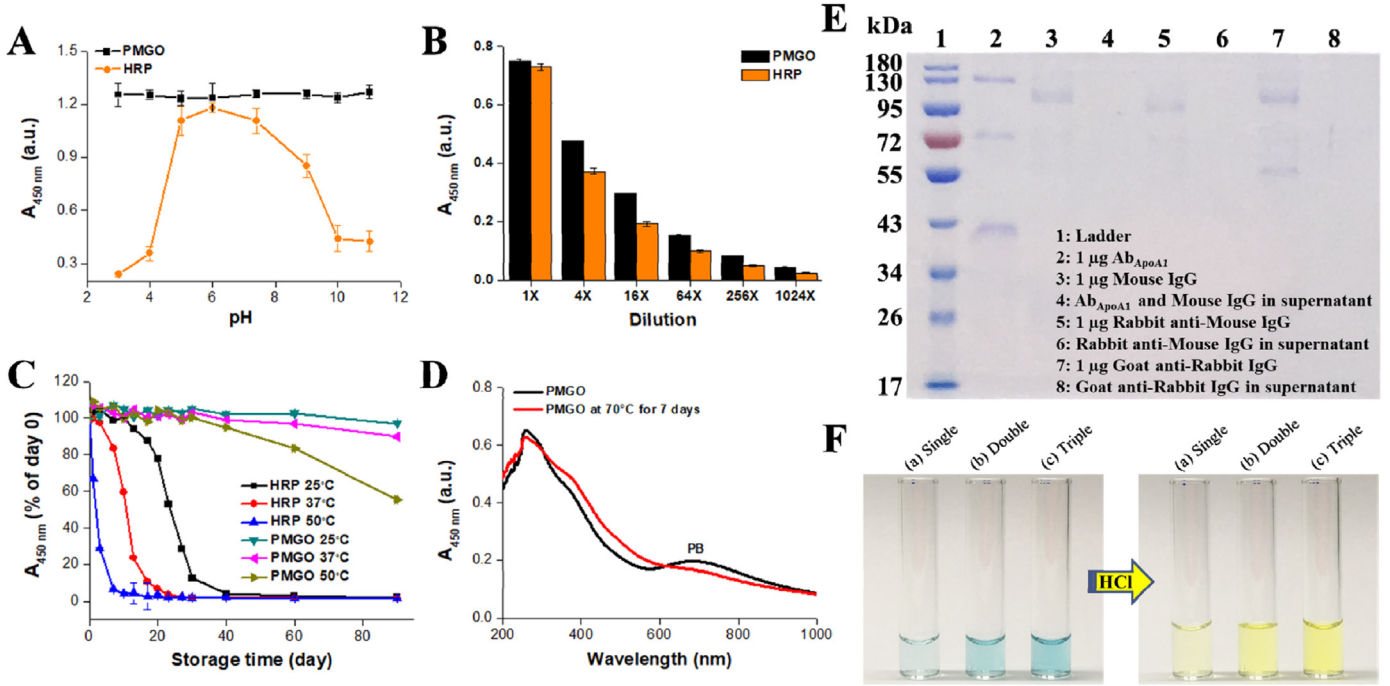

Fig. 4. (A) Absorbance at 450 nm of PMGO and HRP in the presence H_2O_2 + TMB in PBS with different pH levels (n = 3). (B) Comparison of the oxidization of PMGO and HRP with different dilutions to H_2O_2 + TMB (n = 3). (C) Stability of HRP and PMGO stored at 25, 37, and 50 °C for a period of 1–90 days. The PMGO showed no decrease in oxidizability toward H_2O_2 + TMB after 90 days of storage at 37 °C (n = 3). (D) UV–vis spectra of PMGO after 7 days of storage at 70 °C. The results showed that the absorption peak at 680 nm attributed to PB disappeared (n = 3). (E) Analysis of the successful conjugation of different antibodies (AbApoA1, mouse IgG, rabbit anti-mouse IgG, and goat anti-rabbit IgG) on the PMGO surface to form PMGO-1, PMGO-2, and PMGO-3 by SDS-PAGE Gel 12%. (F) Digital photos showing the color change with self-linkable PMGO for signal amplification.

3.5. Specificity of ApoA1 protein in spiked urine sample

During the interference study, we incubated a biochip with typical interfering species and other cancer biomarkers that exist in human plasma or urine, including urea, AA, VEGF, CA19-9, MUC1, FXYD3, BSA, and FBS. In our sensing system, the biochip could specifically capture the target protein (ApoA1) and prevent nonspecific adsorption of other species or self-linkable PMGO on the surface to induce unwanted interference. No obvious $A_{450\ nm}$ was observed when the interfering species were incubated with the biochip and then self-linkable PMGOs were added for signal induction. By contrast, a significant absorbance intensity at 450 nm was observed when 20 ng/mL of ApoA1 was added for incubation with the biochip in the presence of self-linkable PMGOs (Fig. S3), indicating the PMGO-1 would only bind onto ApoA1 to induce self-chain reaction with PMGO-2 and PMGO-3 for signal amplification. To prove the accuracy of our immunosensing system for ApoA1 detection, we spiked various concentrations of ApoA1 into human urine, ranging from 20 ng/mL to 100 ng/mL, and the $A_{450\ nm}$ was recorded; the results are presented in Table S1. The recovery rates of ApoA1 were found to be acceptable and in the range of 98.1–104.7%, and the relative standard deviation was lower than 3%, indicating that our immunosensing system is accurate enough for ApoA1 detection. As a result, we confirmed that the immunosensing system with self-linkable PMGO for signal amplification in ApoA1 detection had high sensitivity, selectivity, and accuracy.

3.6. Real urine sample test from BC patients

ApoA1 has been identified to be a potential biomarker for early diagnosis and clinical classification of BC with a sensitivity and specificity of 89.2% and 84.6%, respectively (Li et al., 2014). The urine samples of aggressive BC showed significant increases in ApoA1 expression compared with low malignant BC (Li et al., 2011). A total of sixteen urine samples were collected from the patients diagnosed with BC (ten urine samples from BC patients were collected before surgical operation and chemotherapy; six urine samples from BC patients were collected after surgical operation and chemotherapy) and four healthy people to assess the utility of our immunosensor; the results were also compared with those obtained using a conventional detection method (i.e., an ELISA), and no significant difference was found between them (Fig. 6A). The results indicated that this immunosensor with self-linkable PMGOs for a signal amplification approach potentially offers a more accurate and rapid alternative (within 60 min) than current tests that are based on immunological methods, such as an ELISA, immunohistochemistry, or two-dimensional electrophoresis (2-DE) coupled with mass spectrometry.

The concentrations of ApoA1 in the urine of four healthy people using our immunosensor were 5.1 ± 1.2, 2.2 ± 0.5, 6.5 ± 1.1, and 4.8 ± 0.3 ng/mL, respectively, which were all lower than the cut-off value (11.16 ng/mL). By contrast, the concentrations of ApoA1 were detected using the immunosensor as being between 55.6 ± 2.3 and 104.7 ± 7.4 ng/mL for the patients who were diagnosed with high-grade BC, and between 19.3 ± 4.3 and 22.3 ± 4.9 ng/mL for the patients who were diagnosed with low-grade BC. In addition, we found a notable trend; the ApoA1 concentrations (1.4 ± 0.8 ~ 10.3 ± 1.6 ng/mL) were significantly decreased to normal level in the urine of the patients who were diagnosed with high-grade BC then received surgery and chemotherapy, and no recurrence was observed (Fig. 6B). The report of a pathological section also showed the results were negative for malignancy. Taken together, our colorimetric immunosensor with self-linkable PMGOs for signal amplification can be a potential tool to rapidly and accurately detect ApoA1 concentrations in urine for the early diagnosis, classification of tumor grade, and prognosis monitoring in BC.

4. Conclusion

We successfully developed self-linkable PMGO as a peroxidase-

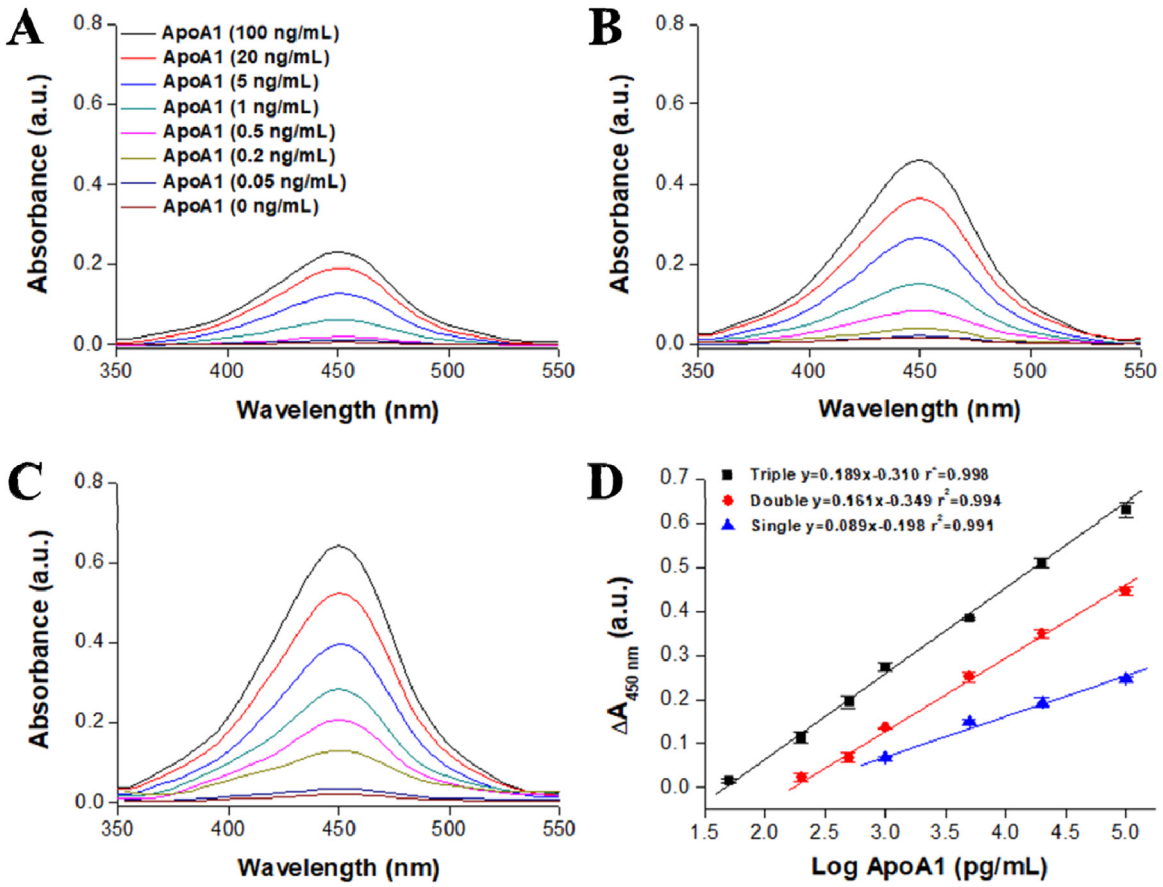

Fig. 5. UV–vis spectra of TMB for the detection of ApoA1 proteins under different conditions: (A) biochip$_{ApoA1}$ + ApoA1 + PMGO-1; (B) biochip$_{ApoA1}$ + ApoA1 + (PMGO-1 + PMGO-2); and (C) biochip$_{ApoA1}$ + ApoA1 + (PMGO-1 + PMGO-2 + PMGO-3). (D) Linear calibration curve between the $\Delta A_{450\ nm}$ against the concentration of ApoA1 (1 ng/mL-100 ng/mL for PMGO-1; 0.2 ng/mL-100 ng/mL for PMGO-1 + PMGO-2; and 0.05 ng/mL-100 ng/mL for PMGO-1 + PMGO-2 + PMGO-3) (n = 6).

mimicking nanozyme for signal amplification to form an ultrasensitive immunosensor with biochip$_{ApoA1}$ for the simple and rapid diagnosis and prognosis monitoring of BC. As a result of this approach, our study demonstrated that the colorimetric immunosensor can accurately detect the ApoA1 concentration in urine as well as an ELISA assay can, and the self-signal amplification strategy can significantly widen the detection range of ApoA1, from 0.05 ng/mL to 100 ng/mL with an LOD of 0.02 ng/mL, which was achieved within a period of 60 min, allowing for the detection of ApoA1 in clinical urine samples. The biosensing of clinical urine samples shows a reasonable variation with a standard reference from the hospital, also confirmed the importance of ApoA1, which can add information regarding the pathophysiological mechanisms of BC. More importantly, our colorimetric immunosensor with self-linkable PMGOs for signal amplification has a simple, convenient, high sensitivity, high selectivity and low cost, providing a promising tool for point-of-care medical diagnosis and prognosis monitoring, and could

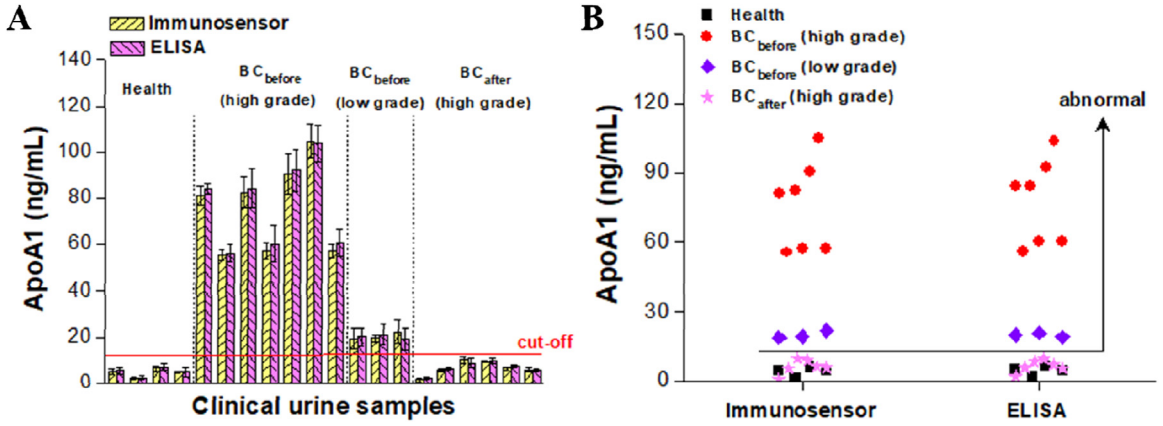

Fig. 6. (A) ApoA1 concentrations in 20 urine samples (4 from healthy people, 14 from BC patients) measured using the immunosensor with self-linkable PMGOs and an ELISA for BC diagnosis and prognosis monitoring (n = 3). (B) The level of ApoA1 in urine samples from healthy people and BC patients detected by immunosensor with self-linkable PMGOs and ELISA for BC diagnosis and prognosis monitoring. BC$_{before}$: the urine from the BC patient collected before treatment; BC$_{after}$: the urine from the BC patient collected after clinical treatment and no recurrence observed.

rival other commercially available instruments in the future.

Acknowledgments

This work was financially supported by the Ministry of Science and Technology (MOST107–2221-E-182-019, MOST106–2628-E-110-001-MY3, MOST106–2628-B-110-001-MY4), Chang Gung Memorial Hospital (CMRPG3D1091-3, CMRPG3D0501-3, CMRPG3D0103, CIRPG3E2041), and Formosa Plastics Corporation (FCRPD2H0011), Taiwan, R.O.C. We would also like to thank the Chang Gung Memorial Hospital Microscopy Core Laboratory for their assistance with TEM and EDS.

Appendix A. Supporting information

Supplementary data associated with this article can be found in the online version at doi:10.1016/j.bios.2018.11.022.

References

Chen, C.L., Lai, Y.F., Tang, P., Chien, K.Y., Yu, J.S., Tsai, C.H., Chen, H.W., Wu, C.C., Chung, T., Hsu, C.W., Chen, C.D., Chang, Y.S., Chang, P.L., Chen, Y.T., 2012. J. Proteome Res. 11, 5611–5629.
Chen, C.L., Lin, T.S., Tsai, C.H., Wu, C.C., Chung, T., Chien, K.Y., Wu, M., Chang, Y.S., Yu, J.S., Chen, Y.T., 2013. J. Proteom. 85, 28–43.
Farka, Z., Čunderlová, V., Horáčková, V., Pastucha, M., Mikušová, Z., Hlaváček, A., Skládal, P., 2018. Anal. Chem. 90, 2348–2354.
Garg, B., Bisht, T., Ling, Y.C., 2015. Molecules 20, 14155–14190.
Hassanzadeh, J., Khataee, A., 2018. Talanta 178, 992–1000.
He, Y., Niu, X., Shi, L., Zhao, H., Li, X., Zhang, W., Pan, J., Zhang, X., Yan, Y., Lan, M., 2017. Microchim. Acta 184, 2181–2189.
Kandimalla, R., Van Tilborg, A.A., Zwarthoff, E.C., 2013. Nat. Rev. Urol. 10, 327–335.
Kang, H.W., Seo, S.P., Jeong, P., Ha, Y.S., Kim, W.T., Kim, Y.J., Lee, S.C., Yun, S.J., Kim, W.J., 2017. Oncol. Lett. 14, 2468–2474.
Kompier, L.C., Lurkin, I., Madelon, N.M.A., Rhijn, B.W.G., Kwast, T.H., Zwarthoff, E.C., 2010. PLoS One 5, e13821.
Leiblich, A., 2017. Curr. Urol. Rep. 18, 100.
Li, C., Li, H., Zhang, T., Li, J., Liu, L., Chang, J., 2014. Biochem. Biophys. Res. Commun. 446, 1047–1052.
Li, H., Li, C., Wu, H., Zhang, T., Wang, J., Wang, S., Chang, J., 2011. Proteome Sci. 9, 21.
Li, X., Li, J., Zhu, C., Zhang, X., Chen, J., 2018. Talanta 182, 292–298.
Liu, S., Xu, N., Tan, C., Fang, W., Tan, Y., Jiang, Y., 2018. Anal. Chim. Acta 1018, 86–93.
Maas, M., Walz, S., Stühler, V., Aufderklamm, S., Rausch, S., Bedke, J., Stenzl, A., Todenhöfer, T., 2018. Expert Rev. Mol. Diagn. 18, 443–455.
Machala, L., Zoppellaro, G., Tuček, J., Šafářová, K., Marušák, Z., Filip, J., Pechoušeka, J., Zbořil, R., 2013. RSC Adv. 3, 19591–19599.
Pichler, R., Tulchiner, G., Fritz, J., Schaefer, G., Horninger, W., Heidegger, I., 2017. Int. J. Med. Sci. 14, 811–819.
Pursey, J.P., Chen, Y., Stulz, E., Park, M.K., Kongsuphol, P., 2017. Sens. Actuator B-Chem. 251, 34–39.
Roberts, W.S., Davis, F., Holmes, J.L., Collyer, S.D., Larcombe, L.D., Morgan, S.L., Higson, S.P., 2013. Biosens. Bioelectron. 41, 282–288.
Shao, C.H., Chen, C.L., Lin, J.Y., Chen, C.J., Fu, S.H., Chen, Y.T., Chang, Y.S., Yu, J.S., Tsui, K.H., Juo, C.G., Wu, K.P., 2017. Oncotarget 8, 38802–38810.
Siegel, R.L., Miller, K.D., Jemal, A., 2018. CA: Cancer J. Clin. 68, 7–30.
Stankovich, S., Dikin, D.A., Piner, R.D., Kohlhaas, K.A., Kleinhammes, A., Jia, Y., Wu, Y., Nguyen, S.T., Ruoff, R.S., 2007. Carbon 45, 1558–1565.
Thomas, S., Hao, L., Ricke, W.A., Li, L., 2016. Proteom. Clin. Appl. 10, 358–370.
Tian, L., Qi, J., Qian, K., Oderinde, O., Cai, Y., Yao, C., Song, W., Wang, Y., 2018a. Sens. Actuator B-Chem. 260, 676–684.
Tian, L., Qi, J., Oderinde, O., Yao, C., Song, W., Wang, Y., 2018b. Biosens. Bioelectron. 110, 110–117.
Tsai, C.H., Chen, Y.T., Chang, Y.H., Hsueh, C., Liu, C.Y., Chang, Y.S., Chen, C.L., Yu, J.S., 2018. Oncotarget 9, 30731–30747.
Yeung, C., Dinh, T., Lee, J., 2014. Pharmacoeconomics 32, 1093–1104.
Yokoi, K., Yamashita, K., Watanabe, M., 2017. Int. J. Mol. Sci. 18, 735.
Zell, M., Husser, C., Staack, R.F., Jordan, G., Richter, W.F., Schadt, S., Pähler, A., 2016. Anal. Chem. 88, 11670–11677.
Zhao, B., Huang, Q., Dou, L., Bu, T., Chen, K., Yang, Q.F., Yan, L.Z., Wang, J.L., Zhang, D.H., 2018. Sens. Actuator B-Chem. 275, 223–229.